

Agent Journey Beyond RGB: Hierarchical Semantic-Spatial Representation Enrichment for Vision-and-Language Navigation

Xuesong Zhang^{1*}, Yunbo Xu^{1*}, Jia Li^{1†}, Ruonan Liu², Zhenzhen Hu¹

¹Hefei University of Technology, Hefei, China

²Shanghai Jiao Tong University, Shanghai, China

{xszhang_hfut, xuyunboen}@mail.hfut.edu.cn, jiali@hfut.edu.cn,
ruonan.liu@sjtu.edu.cn, huzhen.ice@gmail.com

Abstract

Navigating unseen environments based on natural language instructions remains difficult for egocentric agents in Vision-and-Language Navigation (VLN). Intuitively, humans inherently ground concrete semantic knowledge within spatial layouts during indoor navigation. Although previous studies have introduced diverse environmental representations to enhance reasoning, other co-occurrence modalities are often naively concatenated with RGB features, resulting in sub-optimal utilization of each modality's distinct contribution. Inspired by this, we propose a hierarchical Semantic Understanding and Spatial Awareness (SUSA) architecture to enable agents to perceive and ground environments at diverse scales. Specifically, the Textual Semantic Understanding (TSU) module supports local action prediction by generating view-level descriptions, thereby capturing fine-grained environmental semantics and narrowing the modality gap between instructions and environments. Complementarily, the Depth-enhanced Spatial Perception (DSP) module incrementally constructs a trajectory-level depth exploration map, providing the agent with a coarse-grained comprehension of the global spatial layout. Extensive experiments demonstrate that SUSA's hierarchical representation enrichment not only boosts the navigation performance of the baseline on discrete VLN benchmarks (RÉVERIE, R2R, and SOON), but also exhibits superior generalization to the continuous R2R-CE.

Code — <https://github.com/HCI-LMC/VLN-SUSA>

1 Introduction

With the advancement of multimodal technology (Radford et al. 2021; Li et al. 2023a; Zhang et al. 2024) in the artificial intelligence community, embodied VLN tasks (Krantz et al. 2020; Qi et al. 2020; Das et al. 2018) have garnered significant attention due to their promising applications in robotics and intelligent assistance. Conventional VLN tasks (Anderson et al. 2018; Krantz et al. 2020) focused on step-by-step navigation in unseen environments based on detailed instructions, while goal-oriented VLN tasks (Zhu et al. 2021; Qi et al. 2020) demand agents to identify predefined objects based on high-level instructions. Consequently, VLN agents

*These authors contributed equally.

†Corresponding author.

Copyright © 2026, Association for the Advancement of Artificial Intelligence (www.aaai.org). All rights reserved.

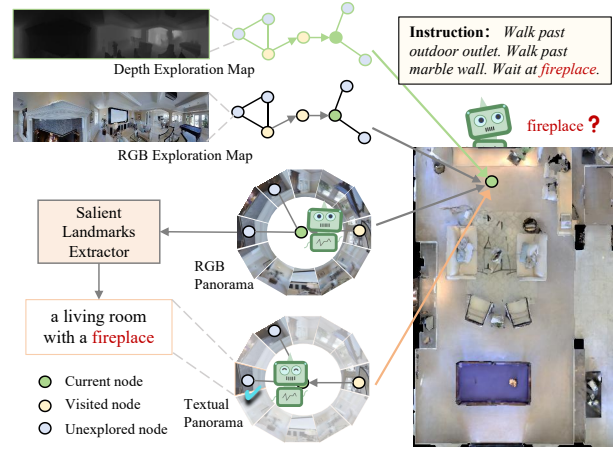


Figure 1: An overview of the proposed SUSA. Beyond RGB inputs, we introduce view-level *textual panoramas* and trajectory-level *depth exploration maps*, supporting the agent's explicit understanding of the environment.

are required to profoundly cognize the environmental spatial information and ground them with textual instructions to brilliantly accomplish navigation tasks.

Recently, increasing the diversity and quantity of augmented environments (Wang et al. 2023b,c; Liu, Wang, and Yang 2024) has emerged as a popular strategy to facilitate the generalization ability of VLN agents in unseen scenarios. This trend is largely motivated by the limited navigational environments in simulators, as well as the powerful fitting capacity of Transformer-based VLN models (Chen et al. 2021; Pashevich, Schmid, and Sun 2021). Nonetheless, VLN agents still struggle to accurately ground the landmarks mentioned in language instructions with the RGB-based visual scene, due to the intrinsic modality heterogeneity. To address this, recent studies introduce textual semantics as perceptual representations to guide navigation (Pan et al. 2024). These approaches leverage candidate object concepts (Wang et al. 2023a; Lin et al. 2023), large language models (LLMs) (Lin et al. 2024), or external knowledge (Li et al. 2023b) to explicitly reason about textual descriptions of landmarks and enhance environmental grounding. However, these methods tend to combine textual and visual rep-

resentations in a straightforward manner, which limits the effective utilization of each modality and constrains the interpretability of their individual contributions. Similarly, co-occurring environmental cues from other modalities—such as frequency (He et al. 2024), spectrum (Hwang et al. 2023), and depth (Tan et al. 2022)—have also been preliminarily explored, though remain underutilized.

In this work, we propose the hierarchical Semantic Understanding and Spatial Awareness (SUSA) architecture, which augments the agent’s environmental comprehension by effectively perceiving and exploiting fine-grained textual semantics and coarse-grained depth-aware spatial information. To enable fine-grained semantic grounding, as shown in Fig. 1, we construct a view-level textual panorama by extracting salient landmarks as textual semantics, thereby bridging the gap between visual and linguistic modalities. The most instruction-relevant view is then selected for local navigation prediction. For global action prediction, we progressively construct a trajectory-level depth exploration map to strengthen the agent’s coarse-grained spatial perception. Finally, SUSA hierarchically aggregates these hybrid semantic-spatial representations to perceive complementary environmental information and employs contrastive learning to align them with natural language instructions. Extensive experiments on four VLN benchmarks (R2R (Anderson et al. 2018), REVERIE (Qi et al. 2020), SOON (Zhu et al. 2021) and R2R-CE (Krantz et al. 2020)) demonstrated the superiority of hybrid semantic-spatial representations enrichment. The contributions of our SUSA are as follows:

- SUSA devises a textual-aware semantic understanding (TSU) module to perceive fine-grained textual semantics of environments, and explicitly address modality heterogeneity between instructions and environments.
- SUSA further constructs a depth exploration map within the depth-enhanced spatial perception (DSP) module to complementarily perceive global environmental layouts and reinforce holistic spatial awareness beyond RGB.
- Experiments demonstrate that SUSA substantially improves upon the baseline, achieving state-of-the-art performance on three discrete VLN tasks, and exhibits promising generalization in continuous environments.

2 Related Work

Vision-and-Language Navigation (VLN). Vision-and-Language Navigation (VLN) tasks (Anderson et al. 2018; Qi et al. 2020; Zhu et al. 2021) require an agent to navigate in embodied environments sequentially towards a designated location or object based on natural language instructions. Given that the VLN task can be formulated as a partially observable Markov decision process, early methods (Wang et al. 2019; Fried et al. 2018) primarily relied on reinforcement learning and imitation learning paradigms to improve navigation performance, incorporating various strategies and auxiliary loss (Wang et al. 2019) designs. More recently, to better model the relationship between the environment and instructions, many researchers (Chen et al. 2021; Pashevich, Schmid, and Sun 2021) have focused on

transformer-based architectures, which effectively model interactions among instructions, environmental features, and historical navigation trajectories.

Environment Representations in VLN. Limited training sources and environmental representations in VLN tasks hinder the agent to generalize the unknown layouts. To alleviate this limitation, recent endeavors (Wang et al. 2023b; Chen et al. 2022a) augment the quantity of environmental scenes, while others diversify environmental representations by constructing graphs (Georgakis et al. 2022; Huang et al. 2023), grids (Wang et al. 2023c; An et al. 2023), or volumetric environments (Liu, Wang, and Yang 2024). Beyond RGB inputs, recent efforts have explored other co-occurrence multimodal(Li et al. 2023b; He et al. 2024) cues to enrich environmental representations. For instance, SEAT (Wang et al. 2024b) enhances cross-domain environmental perception by querying the Matterport3D simulator (Chang et al. 2017) for depth and semantics. However, SEAT fuses these multi-type representations into a unified space without explicitly grounding each modality. Moreover, these semantic representations (Wang et al. 2024b; Hong et al. 2023) are not inherently textual, limiting their ability to bridge the modality gap. Other approaches incorporate depth information (An et al. 2023; Wang et al. 2023c); however, they typically project depth values onto the spatial coordinates of RGB images without independently grounding the depth modality. In contrast, our method constructs the view-level textual panoramas and trajectory-level depth exploration maps, individually grounding them with instructions to perceive rich environmental representations.

3 Methodology

3.1 Preliminary

Task Formulation. We focus on discrete VLN tasks (Anderson et al. 2018; Qi et al. 2020; Zhu et al. 2021) within a Matterport3D simulator (Chang et al. 2017), modeled as an undirected graph $\mathcal{G} = \{\mathcal{N}, \mathcal{E}\}$, where \mathcal{N} denotes nodes and \mathcal{E} signifies the connectivity paths. At the outset of each episode, the agent equipped with a GPS sensor, RGB and depth cameras, is situated at a randomly navigable node and receives a language instruction $I = \{w_i\}_{i=1}^l$ including l words. We use BERT (Devlin et al. 2019) to extract instruction features and then embed them as $\mathcal{I} = \{w_1, \dots, w_l\}$. At each time step t , the agent can perceive the surrounding RGB panorama $R_t = \{r_{t,i}\}_{i=1}^{n=36}$ and depth panorama $D_t = \{d_{t,i}\}_{i=1}^{n=36}$ along with n corresponding views. During navigation, the agent makes the next action a_t by selecting one navigable node from the candidate actions $\mathcal{A}_t = \{a_{t,i}\}_{i=0}^k$.

Overview of the Proposed Method. Our objective is to enrich complementary environmental content by equipping the agent with a textual semantic panorama and a depth exploration map. Following prevailing approaches (He et al. 2024), we adopt DUET (Chen et al. 2022b) as our baseline, which merely utilizes RGB panoramas and topological maps as environmental representations for both local and global action predictions. The SUSA framework consists of three main modules: (a) *TSU*: textual-aware semantic selection is detailed in Section 3.2, (b) *DSP*: depth-enhanced visual en-

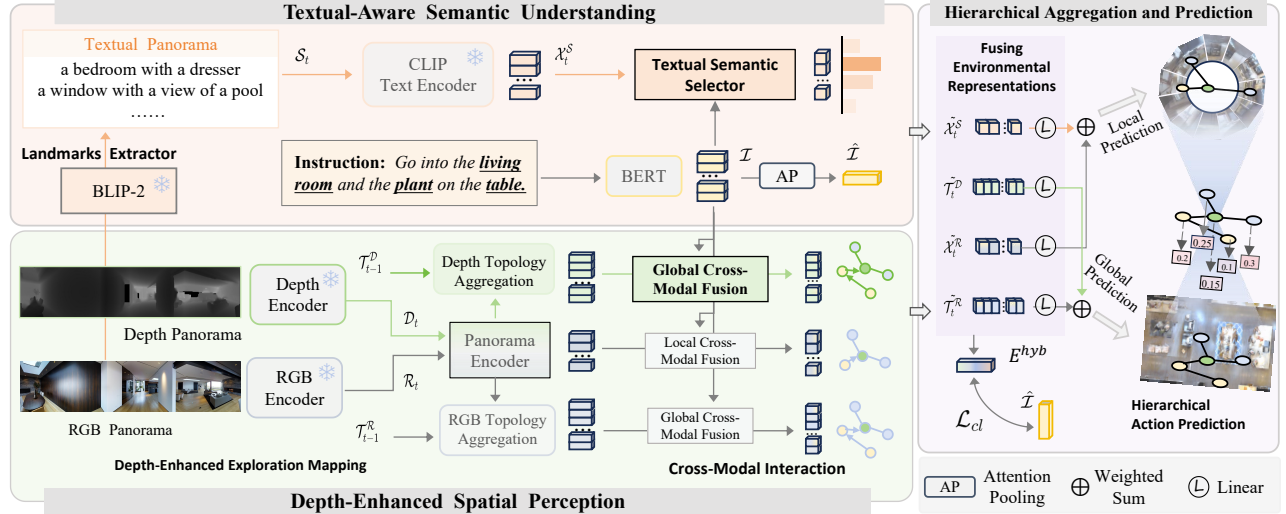


Figure 2: The detailed architecture of our proposed SUSA model. The orange and green arrows highlight our proposed Textual-Aware Semantic Understanding (TSU) and Depth-Aware Spatial Perception (DSP) modules, respectively. The Hierarchical Aggregation and Prediction (HAP) module is designed for hierarchical aligning environmental representations with instructions.

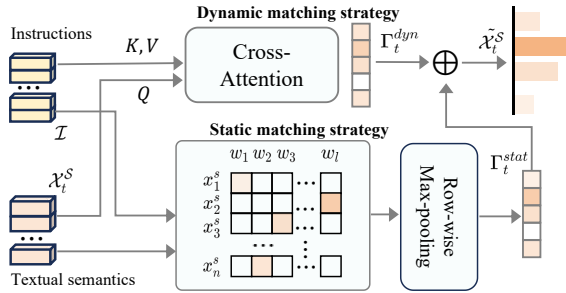


Figure 3: Illustration of the *TSU* module in Fig.2, which matches instructions and semantic features by static and dynamic matching strategies.

vironment exploration is presented in Section 3.3, and (c) *HAP*: hybrid representation aggregation and hierarchical action prediction is subsequently introduced in Section 3.4, as illustrated in Fig. 2.

3.2 Textual-Aware Semantic Understanding

In this module, we build a textual semantic panorama that enables the agent to understand the environment from a textual perspective, allowing it to select the most relevant navigable view as the optimal local navigation action.

Salient Landmarks Extractor. The pretrained visual-language model readily provides the capability for agents to perceive textual semantics by generating detailed captions from RGB images. As illustrated in Fig. 2, we utilize off-the-shelf BLIP-2-FlanT5-xxL (Li et al. 2023a), a powerful visual-language model, to discretize R_t and generate corresponding textual descriptions for each view using the simple prompt “a photo of”. Following (Gao et al. 2024; Li and Bansal 2023), this process yields a textual panorama

$\mathcal{S}_t = \{s_{t,i}\}_{i=1}^{n=36}$, where each view $s_{t,i}$ contains informed descriptions of salient landmarks. These descriptions typically involve room types and objects (e.g., “a living room with two chairs”), which assist in the object recognition. We further discuss the quality of the generated descriptions in supplementary materials. Additionally, we employ the CLIP (ViT-L-14-336px) text encoder (Radford et al. 2021) to extract textual semantic panorama features, embedding them as $\mathcal{X}_t^S = \{x_{t,1}^S, \dots, x_{t,n}^S\}$. Thanks to the powerful yet frozen BLIP-2 and CLIP models, we empower the agent to obtain textual semantic features from the navigable nodes in its vicinity during navigation.

Textual Semantic Selector. Similar to (Pan et al. 2024), we treat the textual semantic as a perceptual representation for navigation in this module, directly matching salient landmarks with the instructions. As shown in Fig. 2 and Fig. 3, our textual semantic selector combines both *static* and *dynamic* matching strategies to select the most instruction-relevant view in the textual panorama \mathcal{X}_t^S .

Static Matching: The most straightforward approach to semantic alignment is by calculating similarity, where higher similarity indicates stronger relevance between the textual semantics of each view and the instruction. Consequently, we calculate the cosine similarity matrix $\mathbf{M} \in \mathbb{R}^{n \times l}$, which represents the correlation between each word in the instruction \mathcal{I} and each view in the textual panorama \mathcal{X}_t^S . Nevertheless, the textual semantics generated only correspond to salient landmarks (e.g., “plant,” or “table”) rather than actions (e.g., “go to” or “turn left”) in the instructions. Therefore, we then apply row-wise max-pooling to purify the static instruction relevance $\Gamma_t^{stat} \in \mathbb{R}^n$ to match the most relevant landmarks between textual semantics and instructions at step t :

$$\mathbf{M}_{i,j} = \frac{\mathcal{X}_{t,i}^S \cdot \mathcal{I}_j}{\|\mathcal{X}_{t,i}^S\| \|\mathcal{I}_j\|}, \quad \Gamma_t^{stat} = \max_j \mathbf{M}_{i,j} \quad (1)$$

where $i = 1, \dots, n$ and $j = 1, \dots, l$. Although straightforward, the static strategy relies on the monotonic similarity matrix to match textual semantics \mathcal{X}_t^S and instructions \mathcal{I} , struggling with long-term navigation reasoning.

Dynamic Matching: Furthermore, a dynamic matching strategy is introduced to better capture the intricate relationships between the environment and instruction. Specifically, we utilize a standard multi-layer transformer decoder to dynamically match the relevance Γ_t^{dyn} between textual semantics and instructions, as formalized by:

$$\Gamma_t^{dyn} = \text{TCA}(\mathcal{X}_t^S, \mathcal{I}, \mathcal{I}), \quad (2)$$

where TCA denotes a textual modality cross-attention mechanism that models textual semantic-instruction relationships. TCA comprises a cross-attention layer, a feed-forward network (FFN) layer, and LayerNorm, enabling the agent to adapt to long-term navigation sequences.

To trade off computational efficiency and navigation accuracy, we flexibly combine the relevance of static Γ_t^{sim} and dynamic Γ_t^{att} . The latent semantic panoramic feature $\tilde{\mathcal{X}}_t^S$ is expressed as follows:

$$\tilde{\mathcal{X}}_t^S = \delta * \Gamma_t^{stat} + (1 - \delta) * \Gamma_t^{dyn}, \quad (3)$$

where the balance factor δ regulates the relative contributions of each matching strategy. By mapping the environment to the same textual modality, the textual semantic selector enables the agent to explicitly understand the environment context from a textual semantic perspective, thus facilitating grounded language instructions.

3.3 Depth-Enhanced Spatial Perception

Depth images, which also contain more intuitive and easily distinguishable structural information, were not adequately exploited in earlier works (Tan et al. 2022). To enhance the spatial perception, we concurrently construct a depth-based exploration map to memorize depth-based navigation trajectory alongside the RGB-based one (Chen et al. 2022b).

Depth-Enhanced Exploration Mapping. Concretely, we obtain ground truth depth images for each view from the Matterport3D simulator. As illustrated in Fig. 2, we then employ ResNet-50 (He et al. 2016) (pretrained on the Gibson (Xia et al. 2018)) and CLIP (ViT-L/14@336px) as the depth and RGB encoders, respectively, to extract panoramic depth features $\mathcal{D}_t \in \mathbb{R}^{n \times d_v}$ and panoramic RGB features $\mathcal{R}_t \in \mathbb{R}^{n \times d_v}$, where d_v represents the dimension of each view. Moreover, we employ a two-layer transformer-based panorama encoding module to perform self-attention and sequentially encode the depth and RGB panoramic images. The panorama encoding modules for both modalities share weights, since each view in the depth and RGB panoramas is accordant. Subsequently, we aggregate each visited node and its adjacent views by average pooling to construct depth and RGB exploration maps in parallel. The explored depth and RGB trajectory maps are formalized as $\mathcal{T}_t^D \in \mathbb{R}^{k \times d_n}$ and $\mathcal{T}_t^R \in \mathbb{R}_t^{k \times d_n}$. Here, k denotes the number of navigable nodes at step t , while d_n represents the dimension of each navigable node. These exploration maps memorize the agent navigation trajectory information for global action

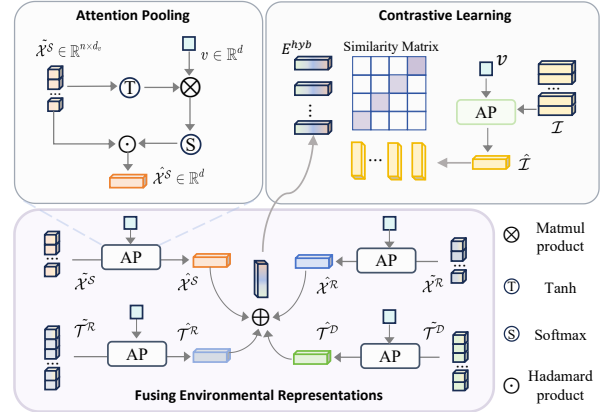


Figure 4: The pipeline for fusing hybrid environmental representations in the proposed HAP module in Fig. 2.

predictions, which serve to guide the agent traversal across various navigable nodes when considering backtracking.

Cross-Modal Interaction and Reasoning. To defer to instructions, we utilize a multi-layer cross-encoder that interacts with both the language instructions and the depth exploration map features to generate the refined depth map $\tilde{\mathcal{T}}^D$. This encoder comprises four residual connection layers of a cross-modal transformer, each incorporating graph-aware self-attention (GASA) (Chen et al. 2022b), cross-modal attention, and a feed-forward network. The GASA operation is formally expressed as $\text{GASA}(X) = \tilde{\mathcal{O}}(X\Theta_q(X\Theta_k)^T + \mathcal{M})X\Theta_v$ where \mathcal{M} represents a learnable distance matrix encoding the relative distances between navigation nodes, $\tilde{\mathcal{O}}$ denotes the Softmax activation function, and $\Theta_q, \Theta_k, \Theta_v$ are learnable weight matrices. In parallel, we facilitate similar cross-modal interactions between the language instructions and the RGB exploration map \mathcal{T}^R , as well as the RGB panoramas \mathcal{X}^R . These are encoded as $\tilde{\mathcal{T}}^R$ and $\tilde{\mathcal{X}}^R$, thereby enabling the model to perform both global and local predictions based on the given instructions \mathcal{I} . Compared to the standalone \mathcal{T}^R , the incorporation of a depth exploration map \mathcal{T}^D enhances the perceptual clarity of environmental structures, mitigating the risk of overfitting to RGB-based visual noises (Ilinykh, Emamoor, and Dobnik 2022) or biases (Hu et al. 2019; Wang et al. 2024a).

3.4 Hierarchical Aggregation and Prediction

Building on aforementioned methods, at the current state t , the agent synchronously perceives the environment through multiple modalities—textual semantic, depth, and RGB—at various scales (local and global). To encourage the agent to aggregate complementary context from these hybrid representations, we encode these features into a low-dimensional latent space via attention pooling and apply contrastive learning to align them with the instructions.

Hybrid Representations Aggregation. As depicted in Fig. 4, we employ attention pooling to project all environmental representations at step t , along with the corresponding instruction, into an equivalent dimension d . Specifically,

the attention pooling AP operation is defined as follows:

$$\hat{\mathcal{H}} = \text{AP}(\mathcal{H}, v), \quad \mathcal{H} \in \{\tilde{\mathcal{X}}^S, \tilde{\mathcal{T}}^D, \tilde{\mathcal{X}}^R, \tilde{\mathcal{T}}^R, \mathcal{I}\}, \quad (4)$$

where $v \in \mathbb{R}^d$ denoting the learnable query vector and $\hat{\mathcal{H}} \in \mathbb{R}^d$. The AP operator is given by:

$$\eta = \mathfrak{D}(\tau(\mathcal{H}) \otimes v^\top), \quad \hat{\mathcal{H}} = \tau(\eta \odot \mathcal{H}), \quad (5)$$

with τ representing the \tanh activation function. Subsequently, we perform weighted aggregation of the hybrid environmental representations E^{hyb} , as follows:

$$\mathcal{B} = [\beta_1 \quad \beta_2 \quad \beta_3 \quad \beta_4]^\top = \sigma(\text{FFN}[\tilde{\mathcal{X}}_0^S; \tilde{\mathcal{X}}_0^R; \tilde{\mathcal{T}}_0^D; \tilde{\mathcal{T}}_0^R]) \quad (6)$$

$$E^{\text{hyb}} = [\hat{\mathcal{X}}^S \quad \hat{\mathcal{X}}^R \quad \hat{\mathcal{T}}^D \quad \hat{\mathcal{T}}^R] \cdot \mathcal{B}, \quad (7)$$

where σ stands for the sigmoid activation function, and $[\cdot]$ denotes concatenation.

Hierarchical Action Prediction. We perform hierarchical action prediction by synergistically fusing the prediction scores from multiple branches to capture complementary information. Specifically, the scores for each branch are computed via separate FFN: $P_{\bar{\mathcal{H}}} = \text{FFN}_{\bar{\mathcal{H}}}(\bar{\mathcal{H}})$, where $\bar{\mathcal{H}} = \{x \in \mathcal{H} \mid x \neq \mathcal{I}\}$. Then, we apply weighted fusion to the textual semantic panorama \mathcal{X}^S and the RGB panorama \mathcal{X}^R to make local predictions, along with global predictions derived from exploration maps based on depth \mathcal{T}^D and RGB \mathcal{T}^R , which is formulated as:

$$P_{\mathcal{X}} = \beta_1 P_{\mathcal{X}^S} + \beta_2 P_{\mathcal{X}^R}, \quad (8)$$

$$P_{\mathcal{T}} = \beta_3 P_{\mathcal{T}^D} + \beta_4 P_{\mathcal{T}^R}. \quad (9)$$

We convert local predictions into global actions and predict a_t via dynamic fusing (Chen et al. 2022b) $P_{\mathcal{T}}$ and $P_{\mathcal{X}}$.

3.5 Training

Partially Pretraining. Our pre-training phase followed prior work (Chen et al. 2022b), utilizing auxiliary tasks such as Masked Language Modeling (MLM), Masked Region Classification (MRC), and Single-step Action Prediction (SAP). Object Grounding (OG) task to localize target objects in REVERIE and SOON. Given the sparsity of depth images and textual semantics compared to RGB images, completely pre-training all parameter of SUSA may lead to overfitting and increased training costs. As shown in Fig. 2, only the computation flows indicated by black arrows were pre-trained. The effectiveness of this partial pre-trained strategy is demonstrated in Section 4.3.

Contrastive and Imitation Learning. During fine-tuning, we employ a contrastive learning loss \mathcal{L}_{cl} to align the hybrid environmental representations E^{hyb} with the corresponding instructions \mathcal{I} :

$$\begin{aligned} \mathcal{L}_{cl} = & -\frac{1}{2B} \sum_{i=1}^B \log \frac{\exp((E_i^{\text{hyb}}, \mathcal{I}_i)/t)}{\sum_{j=1}^B \exp((E_i^{\text{hyb}}, \mathcal{I}_j)/t)} \\ & -\frac{1}{2B} \sum_{i=1}^B \log \frac{\exp((\mathcal{I}_i, E_i^{\text{hyb}})/t)}{\sum_{j=1}^B \exp((\mathcal{I}_i, E_j^{\text{hyb}})/t)}, \end{aligned} \quad (10)$$

where B and t represent the batch size and the temperature. Then, we train the model based on hybrid environment representations by performing single-step action prediction (Chen et al. 2021, 2022b) with a contrastive learning loss \mathcal{L}_{cl} . The hybrid single action

prediction loss in imitation learning is computed as $\mathcal{L}_{hsap}^{gt} = \sum_{t=1}^T -\log p(a_t^{gt} | \mathcal{I}, \mathcal{S}_t, \mathcal{D}_{<t}, \mathcal{R}_{<t})$ and $\mathcal{L}_{hsap}^* = \sum_{t=1}^T -\log p(a_t^* | \mathcal{I}, \mathcal{S}_t, \mathcal{D}_{<t}, \mathcal{R}_{<t})$, where a_t^{gt} represents the ground truth action, and a_t^* denotes the pseudo-target action sampled from current exploration map. The final training loss is then expressed as follows:

$$\mathcal{L}_{SUSA} = \lambda_1 \mathcal{L}_{hsap}^{gt} + \mathcal{L}_{hsap}^* + \lambda_2 \mathcal{L}_{cl} \quad (11)$$

where λ_1 and λ_2 denote loss weights.

4 Experiments

4.1 Task Setup and Implementation

Datasets. We mainly evaluate our model on three diverse VLN benchmarks. **R2R** (Anderson et al. 2018) focuses solely on navigation following detailed instructions. **REVERIE** (Qi et al. 2020) requires the agent to recognize the correct object from candidate bounding boxes upon reaching the navigation goal. **SOON** (Zhu et al. 2021) challenges agents to generate candidate bounding boxes using an object detector. Given that discrete agents can serve as planners of ETPNav (An et al. 2024), we also evaluate SUSA on the continuous R2R-CE (Krantz et al. 2020). **R2R-CE** is constructed from the discrete Matterport3D and executed in the continuous Habitat simulator (Savva et al. 2019).

Metrics. We evaluate the navigation performance using standard metrics: Success Rate (SR), Oracle Success Rate (OSR), Navigation Error (NE), and Success Rate weighted by Path Length (SPL). For the REVERIE and SOON tasks, which involve object identification, we also evaluate object grounding metrics: Remote Grounding Success (RGS) and RGS weighted by Path Length (RGSP). Given that **SPL** optimally balances navigation success rate and trajectory length, we employ it as our primary metric.

Implementation Details. Pre-training was performed for 100k iterations with a batch size of 32. Fine-tuning was performed for 25k iterations for VLN tasks. For fine-tuning, we used batch sizes of 4, 8, 2 and 16 for R2R, REVERIE, SOON and R2R-CE, respectively. The default hyperparameters are $\lambda_1 = 0.2$ and $\lambda_2 = 0.8$. The node and view dimensions are identical: $d_v = d_n = d = 768$. We minimized changes to the baseline (**DUET**) (Chen et al. 2022b) settings and used no additional annotations. All experiments were conducted on a **single** NVIDIA RTX 4090 GPU.

4.2 Comparisons with State of the Art

We primarily conduct a comprehensive comparison on three discrete VLN tasks—REVERIE (Qi et al. 2020), R2R (Anderson et al. 2018), and SOON (Zhu et al. 2021). For fairness, we exclude methods that involve pre-exploration (Sigurdsson et al. 2023) or utilize large-scale data augmentation (Wang et al. 2023b). Tables 1 and 2 present a comparative analysis on REVERIE, R2R, and SOON. Our method achieves, and in some cases surpasses, the performance of previous state-of-the-art approaches on various metrics. For instance, SUSA achieves an SPL/RGSP of 41.5%/27.3% on the REVERIE test unseen split, significantly outperforming the baseline (**DUET**) by a large margin of 5.5%/5.3%.

| Methods | REVERIE | | | | | | R2R | | | | | |
|----------------------------|-------------|-------------|-------------|-------------|-------------|-------------|------------|-------------|-----------------|-------------|-------------|-----------------|
| | Val Unseen | | | Test Unseen | | | Val Unseen | | | Test Unseen | | |
| | SR | SPL | RGSPL | SR | SPL | RGSPL | SR | SPL | NE \downarrow | SR | SPL | NE \downarrow |
| RCM (Wang et al. 2019) | 9.2 | 6.9 | 3.8 | 7.8 | 6.6 | 3.1 | 43 | - | 6.0 | 43 | 38 | 6.1 |
| GridMM (Wang et al. 2023c) | 51.3 | 36.4 | 24.5 | 53.1 | 36.6 | 23.4 | 75 | 64 | - | 73 | 62 | - |
| KERM (Li et al. 2023b) | 49.0 | 34.8 | 24.1 | 52.2 | 37.4 | 23.1 | 71.9 | 60.9 | 3.2 | 69.7 | 59.2 | 3.6 |
| AZHP (Zhan et al. 2024) | 49.0 | 36.2 | 24.1 | 52.5 | 36.1 | 22.5 | 71 | 60 | 3.2 | 69 | 59 | 3.4 |
| FDA (He et al. 2024) | 47.5 | 35.9 | 24.3 | 49.6 | 36.4 | 22.0 | 72 | 64 | 3.4 | 69 | 62 | 3.41 |
| CONSOLE (Lin et al. 2024) | 50.0 | 34.4 | 23.3 | 55.1 | 37.1 | 22.2 | 73 | 63 | 3.0 | 72 | 61 | 3.3 |
| ACME (Wu et al. 2025) | 49.5 | 32.4 | 24.0 | 51.9 | 34.7 | 23.6 | 72.8 | 62.3 | 3.12 | 70.4 | 61.2 | 3.68 |
| DUET (Chen et al. 2022b) | 46.9 | 33.7 | 23.0 | 52.5 | 36.0 | 22.0 | 72 | 60 | 3.3 | 69 | 59 | 3.65 |
| SUSA (Ours) | 51.7 | 38.8 | 26.5 | 54.3 | 41.5 | 27.3 | 73.0 | 64.8 | 3.0 | 72.5 | 63.8 | 3.20 |

Table 1: Comparison with the state of the art on REVERIE and R2R. **Bold** highlights the best performance in each column. \downarrow indicates better performance with lower values. “-”: unavailable statistics. % is omitted for brevity.

| Method | Val Unseen | | Test Unseen | |
|----------------------------|-------------|------------|-------------|------------|
| | SPL | RGSPL | SPL | RGSPL |
| GridMM (Wang et al. 2023c) | 24.8 | 3.9 | 21.2 | 4.1 |
| KERM (Li et al. 2023b) | 23.1 | 4.4 | - | - |
| SEAT (Wang et al. 2024b) | 24.8 | 3.9 | 22.5 | 4.4 |
| ACME (Wu et al. 2025) | 27.8 | 4.3 | 22.3 | 5.5 |
| DUET (Chen et al. 2022b) | 22.5 | 3.7 | 21.4 | 4.1 |
| SUSA(Ours) | 30.8 | 6.4 | 25.4 | 5.9 |

Table 2: Comparison with the state of the art on the SOON.

| Methods | Val Unseen | | Test Unseen | |
|-------------------------------|-------------|-------------|-------------|-------------|
| | SR | SPL | SR | SPL |
| GridMM (Wang et al. 2023c) | 49 | 41 | 46 | 39 |
| AO-Planner (Chen et al. 2025) | 47 | 33 | - | - |
| ETPNav (An et al. 2024) | 57 | 49 | 55 | 48 |
| DUET (Chen et al. 2022b) | 51.9 | 41.2 | 47.1 | 40.5 |
| SUSA (Ours) | 52.7 | 43.6 | 50.9 | 43.9 |

Table 3: Comparison with the state of the art on R2R-CE. We directly transfer the DUET and SUSA as planners of ETPNav into the continuous environment without pretraining. Underline indicates improvements over the baseline.

Furthermore, we briefly transfer the agent into continuous environments to coarsely assess its adaptability and generalization. Results in Table 3 indicate that SUSA achieves superior performance over the baseline in the continuous R2R-CE task, highlighting the potential of hierarchical representation enrichment in continuous navigation scenarios.

4.3 Diagnostic Experiment

1) Image Features vs. Structural Features. We analyze RGB and depth features contributions within the DSP module (Table 4). For RGB images, substituting ViT (Dosovitskiy et al. 2020) features with those from CLIP (Radford et al. 2021) yields marked improvements across all metrics. As for depth features, we leveraged depth features ex-

| RGB | Depth | REVERIE | | R2R | | |
|------|------------|-------------|-------------|-------------|-------------|--|
| | | SR | SPL | RGS | RGSPL | |
| ViT | <i>w/o</i> | 46.9 | 33.7 | 32.1 | 23.0 | |
| CLIP | <i>w/o</i> | 51.5 | 35.7 | 35.1 | 24.4 | |
| CLIP | ImageNet | 50.1 | 34.6 | 34.3 | 23.6 | |
| CLIP | Gibson | 52.0 | 39.2 | 35.0 | 26.5 | |

Table 4: Ablation of different visual representations on the REVERIE validation unseen split. Gibson and ImageNet serve as pre-training sources for the depth encoder (ResNet-50) in the DSP module.

| δ | REVERIE | | | R2R | | |
|-----------------|-------------|-------------|-------------|-------------|-------------|-------------|
| | SR | SPL | RGSPL | SR | SPL | nDTW |
| <i>w/o</i> | 52.0 | 39.2 | 26.5 | 72.8 | 62.7 | 69.3 |
| 0 | 53.9 | 38.8 | 26.8 | 72.2 | 63.7 | 70.7 |
| 0.5 | 55.0 | 39.5 | 26.7 | 73.0 | 64.8 | 71.0 |
| 1.0 | 53.5 | 37.8 | 25.9 | 72.3 | 62.9 | 69.1 |
| <i>adaptive</i> | 52.4 | 38.2 | 26.2 | 71.9 | 63.1 | 69.9 |

Table 5: Ablation of static and dynamic matching strategies in the TSU module, balanced by the balance factor δ .

tracted by ResNet-50 (He et al. 2016) pre-trained on the ImageNet (Deng et al. 2009) or Gibson (Xia et al. 2018) datasets to investigated the effect of depth exploration maps. Compared to ImageNet, the Gibson simulator provides spatial structural information that serves as valuable navigation priors. Therefore, the ResNet-50 pre-trained on the Gibson yields notable improvements in the SPL metric without compromising SR or RGS. These improvements indicate that better spatial perception enhances navigation efficiency.

2) Static Matching vs. Dynamic Matching. To assess the impact of static matching ($\delta = 0$) and dynamic matching ($\delta = 1$) strategies in the TSU module, we perform ablation studies based on balance factor δ on the R2R and REVERIE. Table 5 summarizes these results, where *w/o* indicates the exclusion of the TSU module. Furthermore, *adaptive* denotes that δ is a learnable parameter which adaptively adjusts

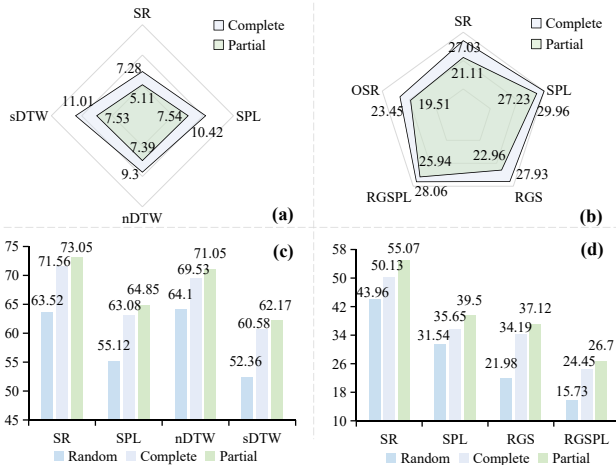


Figure 5: (a) and (b) show the performance gap (↓, lower values indicate better performance.) between seen and unseen environments, while (c) and (d) present key metrics (↑) for different pretraining strategies on the R2R and REVERIE.

| ID | DSP | TSU | HAP | SR | SPL | RGSPL |
|----|-----|-----|-----|------|------|-------|
| 1 | ✗ | ✗ | ✗ | 46.9 | 52.5 | 33.7 |
| 2 | ✓ | ✗ | ✗ | 52.0 | 52.5 | 39.2 |
| 3 | ✗ | ✓ | ✗ | 53.1 | 53.8 | 38.3 |
| 4 | ✓ | ✓ | ✗ | 55.0 | 51.9 | 39.5 |
| 5 | ✓ | ✓ | ✓ | 51.7 | 54.3 | 38.8 |

Table 6: Ablation study on different components of SUSA on the REVERIE (validation|test) unseen split.

the contribution of each matching strategy. While the TSU module can achieve superior performance under the *adaptive* setting, it underperforms when $\delta = 0.5$. Specifically, at $\delta = 0.5$, the SPL reaches 39.50% and 64.85% on the two datasets. Excellent results demonstrate dual merits of TSU module, which boosts object identification accuracy on the REVERIE while simultaneously improving the fidelity between navigation trajectories and instructions on the R2R.

3) Improved Generalization via Pretraining. As aforementioned in Section 3.5, pretraining the entire SUSA framework on multiple auxiliary tasks may lead to overfitting, which negatively impact the generalization in unseen environments. As shown in Fig. 5, the partial pretraining strategy not only consistently narrows the performance gap between seen and unseen environments but also outperforms complete/random pretraining strategies in navigation performance. In Fig. 5 (a), the partial pretraining model achieves an SR gap of only 21.11% between the seen and unseen splits on REVERIE, reducing the gap by 5.92% compared to the complete pretraining strategy. Additionally, as depicted in Fig. 5 (c), multiple metrics indicate that partial pretraining results in superior performance. Fig. 5 (b) and (d) illustrate similar trends are observed on R2R, further emphasizing the generalization of the partial pretraining strategy.

4) Overall Design. To thoroughly evaluate the efficacy of key components, we conduct ablation experiments on

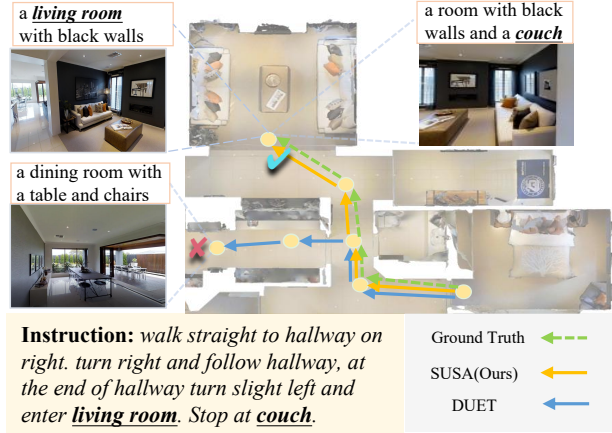


Figure 6: Predicted trajectories of SUSA and DUET on the R2R validation unseen split.

the REVERIE validation and test unseen splits in Table 6. An intriguing phenomenon is observed in Table 6: directly incorporating the DSP and TSU modules (#4) results in an improvement on validation unseen (e.g., SR=55.07, SPL=39.50), while performance on test unseen deteriorates. Conversely, contrastive learning within the HAP module (#5) produces opposite outcomes, particularly with respect to the SR metric. This may be attributed to the learnable token v , which, while pooling hybrid environmental representations, also introduces slight noise that causes fluctuations of navigation performance. Nevertheless, the overall performance is progressively improved with the inclusion of DSP, TSU and HAP modules.

4.4 Qualitative Analysis

As shown in Fig. 6, compared to DUET, our SUSA agent is able to accurately stop near the “living room with a couch.” In contrast, the DUET agent, which relies exclusively on RGB environment representations, is prone to making elusive actions, hindering its ability to accurately follow instructions and reach the target location. This manifests that, thanks to the salient landmarks provided by the SUSA architecture, the agent is better able to navigate to the target location by grounding textual instructions.

5 Conclusion

We present the SUSA architecture, which hierarchical exploits semantic-spatial representations beyond RGB to facilitate environmental understanding and instruction grounding. Specifically, we propose the TSU module, enabling the agent to identify the most instruction-relevant textual semantic. The DSP module complementarily enhances spatial awareness by incrementally constructing and grounding depth exploration maps. Experimental results on the R2R, REVERIE, SOON and R2R-CE benchmarks demonstrate the navigational superiority of our approach. Benefiting from hierarchical representation enrichment and alignment, SUSA exhibits excellent generalization performance on unseen environments and modality interpretability.

6 Acknowledgments

This work was supported by the National Natural Science Foundation of China (NSFC) under Grants Nos. 62202139, 62573292 and 62172138, and also supported by the Fundamental Research Funds for the Central Universities under Grants Nos. JZ2025HGTB0226, JZ2024HGTG0310 and Young Elite Scientist Sponsorship Program (No. YESS20220409). The computations were performed on the High-Performance Computing (HPC) Platform of Hefei University of Technology.

References

An, D.; Qi, Y.; Li, Y.; Huang, Y.; Wang, L.; Tan, T.; and Shao, J. 2023. Bevbert: Multimodal map pre-training for language-guided navigation. In *Proceedings of the IEEE/CVF International Conference on Computer Vision*, 2737–2748.

An, D.; Wang, H.; Wang, W.; Wang, Z.; Huang, Y.; He, K.; and Wang, L. 2024. Etpnav: Evolving topological planning for vision-language navigation in continuous environments. *IEEE Transactions on Pattern Analysis and Machine Intelligence*.

Anderson, P.; Wu, Q.; Teney, D.; Bruce, J.; Johnson, M.; Sünderhauf, N.; Reid, I.; Gould, S.; and Van Den Hengel, A. 2018. Vision-and-language navigation: Interpreting visually-grounded navigation instructions in real environments. In *Proceedings of the IEEE conference on computer vision and pattern recognition*, 3674–3683.

Chang, A.; Dai, A.; Funkhouser, T.; Halber, M.; Niessner, M.; Savva, M.; Song, S.; Zeng, A.; and Zhang, Y. 2017. Matterport3D: Learning from RGB-D Data in Indoor Environments. *International Conference on 3D Vision (3DV)*.

Chen, J.; Lin, B.; Liu, X.; Ma, L.; Liang, X.; and Wong, K.-Y. K. 2025. Affordances-oriented planning using foundation models for continuous vision-language navigation. In *Proceedings of the AAAI Conference on Artificial Intelligence*, volume 39, 23568–23576.

Chen, S.; Guhur, P.-L.; Schmid, C.; and Laptev, I. 2021. History aware multimodal transformer for vision-and-language navigation. *Advances in neural information processing systems*, 34: 5834–5847.

Chen, S.; Guhur, P.-L.; Tapaswi, M.; Schmid, C.; and Laptev, I. 2022a. Learning from unlabeled 3d environments for vision-and-language navigation. In *European Conference on Computer Vision*, 638–655. Springer.

Chen, S.; Guhur, P.-L.; Tapaswi, M.; Schmid, C.; and Laptev, I. 2022b. Think global, act local: Dual-scale graph transformer for vision-and-language navigation. In *Proceedings of the IEEE/CVF Conference on Computer Vision and Pattern Recognition*, 16537–16547.

Das, A.; Datta, S.; Gkioxari, G.; Lee, S.; Parikh, D.; and Batra, D. 2018. Embodied Question Answering. In *Proceedings of the IEEE Conference on Computer Vision and Pattern Recognition (CVPR)*.

Deng, J.; Dong, W.; Socher, R.; Li, L.-J.; Li, K.; and Fei-Fei, L. 2009. Imagenet: A large-scale hierarchical image database. In *2009 IEEE conference on computer vision and pattern recognition*, 248–255. Ieee.

Devlin, J.; Chang, M.-W.; Lee, K.; and Toutanova, K. 2019. Bert: Pre-training of deep bidirectional transformers for language understanding. In *Proceedings of the 2019 conference of the North American chapter of the association for computational linguistics: human language technologies, volume 1 (long and short papers)*, 4171–4186.

Dosovitskiy, A.; Beyer, L.; Kolesnikov, A.; Weissenborn, D.; Zhai, X.; Unterthiner, T.; Dehghani, M.; Minderer, M.; Heigold, G.; Gelly, S.; et al. 2020. An Image is Worth 16x16 Words: Transformers for Image Recognition at Scale. In *International Conference on Learning Representations*.

Fried, D.; Hu, R.; Cirik, V.; Rohrbach, A.; Andreas, J.; Morency, L.-P.; Berg-Kirkpatrick, T.; Saenko, K.; Klein, D.; and Darrell, T. 2018. Speaker-follower models for vision-and-language navigation. *Advances in Neural Information Processing Systems*, 31.

Gao, F.; Tang, J.; Wang, J.; Li, S.; and Yu, J. 2024. Enhancing Scene Understanding for Vision-and-Language Navigation by Knowledge Awareness. *IEEE Robotics and Automation Letters*.

Georgakis, G.; Schmeckpeper, K.; Wanchoo, K.; Dan, S.; Miltsakaki, E.; Roth, D.; and Daniilidis, K. 2022. Cross-modal map learning for vision and language navigation. In *Proceedings of the IEEE/CVF Conference on Computer Vision and Pattern Recognition*, 15460–15470.

He, K.; Si, C.; Lu, Z.; Huang, Y.; Wang, L.; and Wang, X. 2024. Frequency-Enhanced Data Augmentation for Vision-and-Language Navigation. *Advances in Neural Information Processing Systems*, 36.

He, K.; Zhang, X.; Ren, S.; and Sun, J. 2016. Deep residual learning for image recognition. In *Proceedings of the IEEE conference on computer vision and pattern recognition*, 770–778.

Hong, Y.; Zhou, Y.; Zhang, R.; Dernoncourt, F.; Bui, T.; Gould, S.; and Tan, H. 2023. Learning navigational visual representations with semantic map supervision. In *Proceedings of the IEEE/CVF International Conference on Computer Vision*, 3055–3067.

Hu, R.; Fried, D.; Rohrbach, A.; Klein, D.; Darrell, T.; and Saenko, K. 2019. Are You Looking? Grounding to Multiple Modalities in Vision-and-Language Navigation. In *Proceedings of the 57th Annual Meeting of the Association for Computational Linguistics*, 6551–6557.

Huang, C.; Mees, O.; Zeng, A.; and Burgard, W. 2023. Visual language maps for robot navigation. In *2023 IEEE International Conference on Robotics and Automation (ICRA)*, 10608–10615. IEEE.

Hwang, M.; Jeong, J.; Kim, M.; Oh, Y.; and Oh, S. 2023. Meta-explore: Exploratory hierarchical vision-and-language navigation using scene object spectrum grounding. In *Proceedings of the IEEE/CVF Conference on Computer Vision and Pattern Recognition*, 6683–6693.

Ilinykh, N.; Emamoor, Y.; and Dobnik, S. 2022. Look and answer the question: On the role of vision in embodied ques-

tion answering. In *Proceedings of the 15th International Conference on Natural Language Generation*, 236–245.

Krantz, J.; Wijmans, E.; Majundar, A.; Batra, D.; and Lee, S. 2020. Beyond the Nav-Graph: Vision and Language Navigation in Continuous Environments. In *European Conference on Computer Vision (ECCV)*.

Li, J.; and Bansal, M. 2023. Panogen: Text-conditioned panoramic environment generation for vision-and-language navigation. *Advances in Neural Information Processing Systems*, 36: 21878–21894.

Li, J.; Li, D.; Savarese, S.; and Hoi, S. 2023a. Blip-2: Bootstrapping language-image pre-training with frozen image encoders and large language models. In *International conference on machine learning*, 19730–19742. PMLR.

Li, X.; Wang, Z.; Yang, J.; Wang, Y.; and Jiang, S. 2023b. Kerm: Knowledge enhanced reasoning for vision-and-language navigation. In *Proceedings of the IEEE/CVF Conference on Computer Vision and Pattern Recognition*, 2583–2592.

Lin, B.; Nie, Y.; Wei, Z.; Zhu, Y.; Xu, H.; Ma, S.; Liu, J.; and Liang, X. 2024. Correctable Landmark Discovery Via Large Models for Vision-Language Navigation. *IEEE Transactions on Pattern Analysis and Machine Intelligence*.

Lin, B.; Zhu, Y.; Liang, X.; Lin, L.; and Liu, J. 2023. Actional atomic-concept learning for demystifying vision-language navigation. In *Proceedings of the AAAI Conference on Artificial Intelligence*, volume 37, 1568–1576.

Liu, R.; Wang, W.; and Yang, Y. 2024. Volumetric environment representation for vision-language navigation. In *Proceedings of the IEEE/CVF Conference on Computer Vision and Pattern Recognition*, 16317–16328.

Pan, B.; Panda, R.; Jin, S.; Feris, R.; Oliva, A.; Isola, P.; and Kim, Y. 2024. LangNav: Language as a Perceptual Representation for Navigation. In *Findings of the Association for Computational Linguistics: NAACL 2024*, 950–974.

Pashevich, A.; Schmid, C.; and Sun, C. 2021. Episodic transformer for vision-and-language navigation. In *Proceedings of the IEEE/CVF International Conference on Computer Vision*, 15942–15952.

Qi, Y.; Wu, Q.; Anderson, P.; Wang, X.; Wang, W. Y.; Shen, C.; and Hengel, A. v. d. 2020. Reverie: Remote embodied visual referring expression in real indoor environments. In *Proceedings of the IEEE/CVF Conference on Computer Vision and Pattern Recognition*, 9982–9991.

Radford, A.; Kim, J. W.; Hallacy, C.; Ramesh, A.; Goh, G.; Agarwal, S.; Sastry, G.; Askell, A.; Mishkin, P.; Clark, J.; et al. 2021. Learning transferable visual models from natural language supervision. In *International conference on machine learning*, 8748–8763. PMLR.

Savva, M.; Kadian, A.; Maksymets, O.; Zhao, Y.; Wijmans, E.; Jain, B.; Straub, J.; Liu, J.; Koltun, V.; Malik, J.; et al. 2019. Habitat: A platform for embodied ai research. In *Proceedings of the IEEE/CVF international conference on computer vision*, 9339–9347.

Sigurdsson, G. A.; Thomason, J.; Sukhatme, G. S.; and Pi-ramuthu, R. 2023. Rex-bot: Remote referring expressions with a bag of tricks. In *2023 IEEE/RSJ International Conference on Intelligent Robots and Systems (IROS)*, 5203–5210. IEEE.

Tan, S.; Ge, M.; Guo, D.; Liu, H.; and Sun, F. 2022. Depth-aware vision-and-language navigation using scene query attention network. In *2022 International Conference on Robotics and Automation (ICRA)*, 9390–9396. IEEE.

Wang, L.; He, Z.; Dang, R.; Shen, M.; Liu, C.; and Chen, Q. 2024a. Vision-and-Language Navigation via Causal Learning. In *Proceedings of the IEEE/CVF Conference on Computer Vision and Pattern Recognition*, 13139–13150.

Wang, L.; He, Z.; Tang, J.; Dang, R.; Wang, N.; Liu, C.; and Chen, Q. 2023a. A Dual Semantic-Aware Recurrent Global-Adaptive Network For Vision-and-Language Navigation. In *IJCAI*.

Wang, L.; Tang, J.; He, Z.; Dang, R.; Liu, C.; and Chen, Q. 2024b. Enhanced Language-guided Robot Navigation with Panoramic Semantic Depth Perception and Cross-modal Fusion. In *2024 IEEE/RSJ International Conference on Intelligent Robots and Systems (IROS)*, 7726–7733. IEEE.

Wang, X.; Huang, Q.; Celikyilmaz, A.; Gao, J.; Shen, D.; Wang, Y.-F.; Wang, W. Y.; and Zhang, L. 2019. Reinforced cross-modal matching and self-supervised imitation learning for vision-language navigation. In *Proceedings of the IEEE/CVF conference on computer vision and pattern recognition*, 6629–6638.

Wang, Z.; Li, J.; Hong, Y.; Wang, Y.; Wu, Q.; Bansal, M.; Gould, S.; Tan, H.; and Qiao, Y. 2023b. Scaling data generation in vision-and-language navigation. In *Proceedings of the IEEE/CVF International Conference on Computer Vision*, 12009–12020.

Wang, Z.; Li, X.; Yang, J.; Liu, Y.; and Jiang, S. 2023c. Gridmm: Grid memory map for vision-and-language navigation. In *Proceedings of the IEEE/CVF International Conference on Computer Vision*, 15625–15636.

Wu, J.; Wu, C.; Shen, X.; and Wang, L. 2025. Adaptive Cross-Modal Experts Network with Uncertainty-Driven Fusion for Vision-Language Navigation. *Knowledge-Based Systems*, 307: 112735.

Xia, F.; Zamir, A. R.; He, Z.; Sax, A.; Malik, J.; and Savarese, S. 2018. Gibson env: Real-world perception for embodied agents. In *Proceedings of the IEEE conference on computer vision and pattern recognition*, 9068–9079.

Zhan, Z.; Qin, J.; Zhuo, W.; and Tan, G. 2024. Enhancing Vision and Language Navigation with Prompt-based Scene Knowledge. *IEEE Transactions on Circuits and Systems for Video Technology*.

Zhang, X.; He, J.; Zhao, J.; Hu, Z.; Yang, X.; Li, J.; and Hong, R. 2024. Exploring and exploiting model uncertainty for robust visual question answering. *Multimedia Systems*, 30(6): 1–14.

Zhu, F.; Liang, X.; Zhu, Y.; Yu, Q.; Chang, X.; and Liang, X. 2021. Soon: Scenario oriented object navigation with graph-based exploration. In *Proceedings of the IEEE/CVF Conference on Computer Vision and Pattern Recognition*, 12689–12699.

Appendices

This appendix provides additional materials to complement the main paper. Specifically:

- Section A presents detailed descriptions of metrics, dataset details and pre-training tasks.
- Section B offers extended experimental results, including: (1) comparisons with related approaches, (2) analysis of the learned fusion weights across modalities, (3) evaluation of the quality of generated salient landmarks, (4) ablations on the contrastive loss weight, (5) an overview of the overall design on the R2R benchmark, and (6) a discussion on the trade-off between computational efficiency and navigation performance.
- Section C showcases additional qualitative examples to analyse the agent’s behavior.
- Section D discusses the limitations of our current approach and outlines potential directions for future work.

A Detailed Experimental Setups

Metrics. We categorize the metrics into three types: *Navigation*, *Objects Grounding*, and *Instruction Following*. Detailed calculations of these metrics can be found in Table 7. For *Navigation* metrics, Trajectory Length (TL): Average path length in meters. It is worth noting that since the trajectory needs to match the ground truth trajectory described by the instruction, strictly speaking, the trajectory length is not necessarily the smaller, the better. Success Rate (SR): Proportion of paths where the agent reaches within 3 meters of the target location. Oracle Success Rate (OSR): The proportion of trajectories where at least one node is within 3 meters of a corresponding node in the reference trajectory. Navigation Error (NE): Average final distance (meters) between the agent and the target. Success Rate weighted by Path Length (SPL): Prioritizes success for shorter paths, which normalizes the success rate by trajectory length. For *Instruction Following* metrics, we apply Normalized Dynamic Time Warping (nDTW) and Success Rate Weighted by Dynamic Time Warping (sDTW). The former measures how well the VLN agent could follow the instruction, while the latter considers nDTW for success cases. For *Objects Grounding* metrics: Remote Grounding Success (RGS): Proportion of instructions where the agent correctly identifies the target object. RGS weighted by Path Length (RGSP): Prioritizes correct object identification for shorter paths.

Dataset Details. We primarily evaluate the agent’s navigation capabilities on three distinct VLN datasets: the fine-grained R2R (Anderson et al. 2018), and the goal-oriented REVERIE (Qi et al. 2020) and SOON (Zhu et al. 2021). To further assess generalization in continuous environments (Savva et al. 2019), we extend our evaluation to the R2R-CE (Krantz et al. 2020) task, as shown in Table 8. Each dataset is divided into train, validation seen, validation unseen, and test unseen splits. REVERIE contains approximately 20k high-level instructions describing target locations and objects, with an average instruction length of 21 words. Given predefined object bounding boxes within each panorama, the agent identifies the correct bounding box

| Metric | $\uparrow \downarrow$ | Definition |
|-------------------------------|-----------------------|---|
| <i>Navigation:</i> | | |
| TL | | $\sum_{1 \leq i < P } d(p_i, p_{i+1})$ |
| NE | \downarrow | $d(p_{ P }, g_{ G })$ |
| ONE | \downarrow | $\min_{p \in P} d(p, g_{ G })$ |
| SR | \uparrow | $\mathbb{I}[NE(P, G) \leq d_{th}]$ |
| OSR | \uparrow | $\mathbb{I}[ONE(P, G) \leq d_{th}]$ |
| SPL | \uparrow | $SR(P, G) \cdot \frac{d(p_1, g_{ G })}{\max\{TL(P), d(p_1, g_{ G })\}}$ |
| <i>Instruction Following:</i> | | |
| nDTW | \uparrow | $\exp\left(-\frac{\min_{W \in \mathcal{W}} \sum_{(i_k, j_k) \in W} d(p_{i_k}, q_{j_k})}{ P \cdot d_{th}}\right)$ |
| sDTW | \uparrow | $SR(P, G) * nDTW(P, G)$ |
| <i>Objects Grounding:</i> | | |
| RGS | \uparrow | $\mathbb{I}\left(\max_j IoU(B_i^p, B_j^g) \geq 0.5\right)$ |
| RGSP | \uparrow | $RGS(P, G) \cdot \frac{d(p_1, g_{ G })}{\max\{TL(P), d(p_1, g_{ G })\}}$ |

Table 7: Common VLN metrics, categorized into three types: *Navigation*, *Instruction Following*, and *Object Grounding*. The symbols \uparrow and \downarrow signify if a higher or lower metric value is preferable, respectively. P represents the paths taken by the agent, while G stands for the ground truth trajectories. The function $\mathbb{I}(\cdot)$ serves as an indicator, with $d(n, P)$ measuring the distance from node n to path P , and d_{th} indicating the distance threshold. $W = w_{1..|W|}$ is a warping with $w_k = (i_k, j_k) \in [1 : |P|], [1 : |G|]$, respecting the step-size. B_i^p means the i -th object’s bounding box in agent path (or trajectory).

upon reaching the navigation goal. Unlike the R2R dataset, in the REVERIE task, the agent must identify the correct bounding box from the candidates once the navigation target is reached. R2R includes 22k step-by-step instructions, with an average instruction length of 32 words. The R2R dataset focuses solely on the navigation task, providing detailed path planning for the agent in the instructions. In R2R-CE, the average distance between navigable nodes is significantly shorter compared to R2R (0.19 vs. 2.25 meters), while the number of navigation steps is substantially higher (55 vs. 4–6). SOON is another goal-oriented dataset, containing about 5k instructions, each averaging 47 words in length.

Pre-training Tasks. Following prior works (Chen et al. 2022b, 2021), during pre-training, we employ a suite of multimodal pre-training tasks, including MLM (Masked Language Modeling), MRC (Masked Region Classification), SAP (Single Action Prediction), and OG (Object Grounding). OG is specifically designed for object grounding using the REVERIE and SOON datasets. MLM and MRC aim to establish a robust vision-language alignment. SAP enables the agent to learn preliminary navigation knowledge by predicting the next action during pre-training. However, as navigation is inherently a sequential decision-making process, SAP can only learn static, single-step decisions. When transferring to the R2R-CE task, the agent—serving as part of the

| Dataset | Train | | Val Seen | | Val Unseen | | Test Unseen | | VLN task |
|-----------------------------|-------|-------|----------|-------|------------|-------|-------------|-------|---------------|
| | instr | house | instr | house | instr | house | instr | house | |
| R2R (Anderson et al. 2018) | 14039 | 61 | 1021 | 56 | 2349 | 11 | 4173 | 18 | Fine-grained |
| R2R-CE (Krantz et al. 2020) | 10819 | 61 | 778 | 53 | 1839 | 11 | 3408 | 18 | Fine-grained |
| REVERIE (Qi et al. 2020) | 10466 | 60 | 1423 | 46 | 3521 | 10 | 6292 | 16 | Goal-oriented |
| SOON (Zhu et al. 2021) | 2779 | 34 | 113 | 2 | 339 | 5 | 615 | 14 | Goal-oriented |

Table 8: Comparison of the three VLN datasets utilized in this study.

| Methods | Val Unseen | | | | |
|---------|------------------|--------------|--------------|--------------|--------------|
| | SR | SPL | RGS | RGSPL | |
| Depth | BEVBert | 51.78 | 36.37 | 34.71 | 24.44 |
| | GridMM | 51.37 | 36.47 | 34.57 | 24.56 |
| | SEAT | 49.45 | 35.51 | 32.83 | 23.14 |
| | SUSA(DP) | 52.54 | 37.59 | 35.47 | 25.27 |
| | SUSA(DEM) | 52.00 | 39.21 | 35.05 | 26.54 |
| Text | KESU | 50.36 | 35.15 | 35.02 | 24.17 |
| | KERM | 50.44 | 35.38 | 34.51 | 24.45 |
| | AACL | 49.42 | 33.54 | 33.31 | 22.49 |
| | CONSOLE | 50.07 | 34.40 | 34.05 | 23.33 |
| | SUSA(TP) | 53.17 | 38.31 | 37.18 | 26.73 |

Table 9: Comparison with related works on the REVERIE validation unseen split.

planner module—is not trained from scratch in continuous environments, but only fine-tuned.

We evaluated the experimental results of the unseen test split on the public online leaderboards¹. We assure the readers that we will make our code and model checkpoints publicly available.

B Additional Experiments

B.1 Comparison with Related Approaches

We demonstrate the effectiveness of the proposed method through fair comparisons with related approaches. As shown in Table 9, experiments reveal that directly grounding depth information—whether using depth panoramas (DP) or depth exploration maps (DEM) as input—outperforms prior depth-based methods (An et al. 2023; Wang et al. 2023c, 2024b). Notably, using depth exploration maps leads to better navigation performance than depth panoramas. Similarly, directly aligning textual semantics with instructions via textual panoramas (TP) surpasses methods (Gao et al. 2024; Li et al. 2023b; Lin et al. 2024) that integrate textual semantics into environmental representations. This underscores the superiority of independently grounding each modality, improving the interpretability of each modality’s contribution.

B.2 Fusion Weights of Hybrid Representations.

We quantitatively illustrate the weights (see Eq. 6) assigned to each branch of the HAP module during training (in Fig. 7)

¹<https://eval.ai/web/challenges/challenge-page/606/participate>, <https://eval.ai/web/challenges/challenge-page/97/participate>.

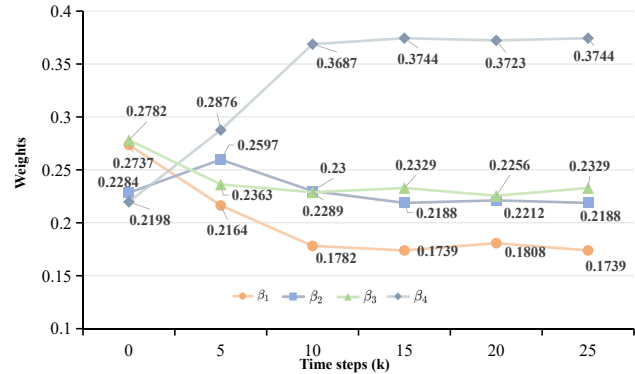


Figure 7: The weights for hybrid representations in the HAP module change during training (see Eq. 6).

| Splits | Local | | Global | |
|------------|-----------|-----------|-----------|-----------|
| | β_1 | β_2 | β_3 | β_4 |
| Val Seen | 0.2147 | 0.2458 | 0.2239 | 0.3156 |
| Val Unseen | 0.2151 | 0.2662 | 0.2216 | 0.2971 |

Table 10: Variation in fusion weights (in Eq. 6) of hybrid representations during inference on R2R. β_1 , β_2 , β_3 , β_4 denotes the fusion weight of textual semantic, local RGB, depth, global RGB representations in the HAP module, respectively.

and inference (in Table 10). These weights are normalized between 0 and 1, with higher values denoting stronger dependency on the corresponding environmental representation. As shown in Fig. 7, initially, all four representations have approximately equal weights of 0.25 during training, reflecting random initialization and balanced contributions. Over the course of training, the global RGB representation weight β_4 increases, while those of the textual semantic β_1 and depth β_3 modalities decrease. This trend arises because textual semantics and depth provide sparse yet precise information, which is particularly beneficial in the early stages of training. Despite the increasing dominance of the RGB modality, the agent’s reliance on textual semantics and depth remains above 20%, underscoring their essential role in navigation. Table 10 also demonstrates that the agent effectively utilizes the introduced depth spatial and textual semantic information during inference, even though it exhibits a stronger reliance on the RGB modality.

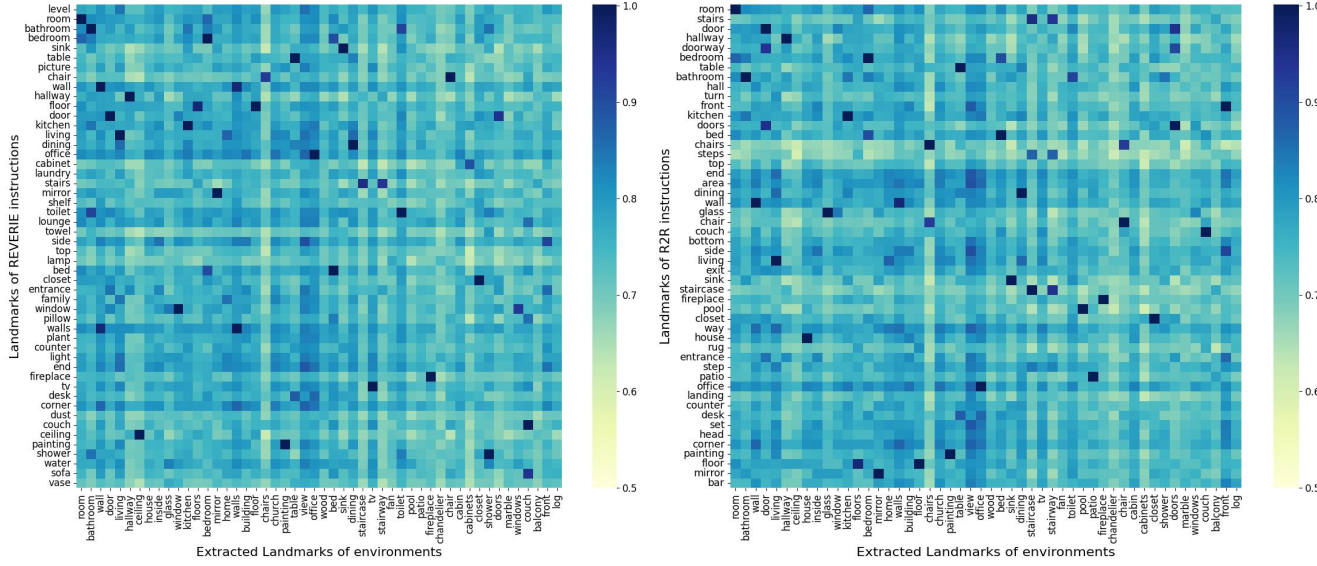


Figure 8: Similarity matrix for the top 50 most frequent landmarks: REVERIE instructions vs. environments (left), R2R instructions vs. environments (right). Best viewed in color.

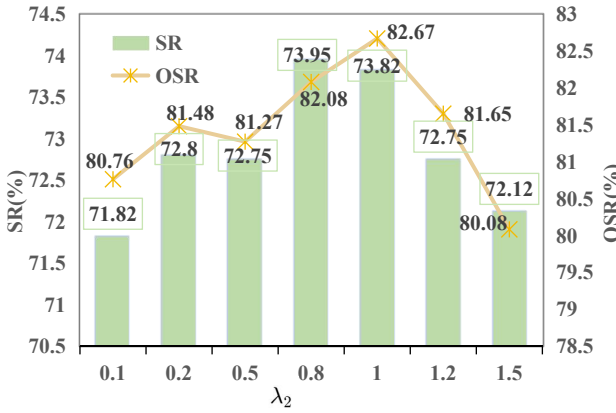


Figure 9: Analysis of the contrastive loss weight λ_2 in HAP module on R2R validation unseen split.

B.3 Quality of Generated Salient Landmarks

The quality of the extracted salient landmarks is crucial for the agent to accurately understand the textual semantics of the environment. In Fig. 8, we compute the similarity between the top-50 most frequently occurring landmarks in our generated salient landmarks and those from R2R (Anderson et al. 2018) and REVERIE (Qi et al. 2020) to evaluate the quality of the generated salient landmarks. While the types and frequencies of these generated landmarks is different from those in the datasets, they can contain and convey most similar semantic (similarities surpass 0.5). Notably, the plug-and-play CLIP text encoder excels in understanding image-related descriptions, while BERT is more adept at comprehending natural language sentences. Therefore, we use the CLIP text encoder to extract features from the gen-

| ID | DSP | TSU | HAP | TL | OSR↑ | SR↑ | SPL↑ |
|----|-----|-----|-----|-------|--------------|--------------|--------------|
| 1 | ✗ | ✗ | ✗ | 13.41 | 79.86 | 71.43 | 60.63 |
| 2 | ✓ | ✗ | ✗ | 13.85 | 80.42 | 72.80 | 62.71 |
| 3 | ✗ | ✓ | ✗ | 13.78 | 81.65 | 72.92 | 63.16 |
| 4 | ✓ | ✓ | ✗ | 12.18 | 79.99 | 73.05 | 64.85 |
| 5 | ✓ | ✓ | ✓ | 14.58 | 82.08 | 73.95 | 62.84 |

Table 11: Ablation study on different components of SUSA on the R2R validation unseen split.

erated salient landmarks.

B.4 Analysis of the Contrastive Loss Weight

Our ablation studies indicate that the contrastive learning loss weight, denoted as λ_2 in Eq. 11, affects model navigation performance. As shown in Fig. 9, agent achieves the optimal navigation performance when the λ_2 is set to 0.8. we further observe that, within a certain range, increasing the contrastive loss weight improves navigation performance. However, when the contrastive loss weight is too high, performance (SR/OSR) declines, thus overemphasizing contrastive learning loss may lead the agent to prioritize modality alignment over core sequential navigation tasks.

B.5 Overall Design on R2R

We further supplemented the performance of each key component of SUSA on the R2R task. As shown in Table 11, our previous conclusions are reaffirmed: the DSP module allows the agent to better perceive spatial layouts, thus improving navigation efficiency (SPL). The TSU module is better at understanding textual semantics, resulting in higher success rates. After integrating the DSP and TSU modules, the agent’s performance improved significantly (e.g., SR=73.05,

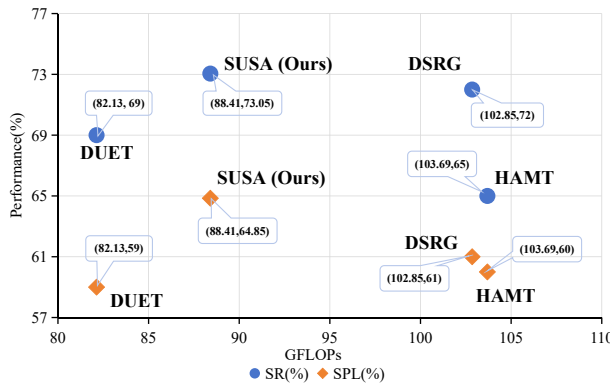


Figure 10: Comparison of computational efficiency and navigation performance on R2R validation unseen split with several popular VLN methods.

SPL=64.85). When the HAP module is further introduced, the navigation success rate on R2R increases to 73.95, indicating that contrastive learning further enhances instruction-environment alignment. However, its SPL metric remains suboptimal, suggesting that the contrastive learning strategy in the HAP module may excel at accurately aligning the environment with instructions but lacks the capability to optimize the navigation path length.

B.6 Computing Efficiency vs. Navigation Performance

As 10 illustrated, we compare the Giga Floating-point Operations (GFLOPs) and navigation performance (i.e, SR/SPL, which are more important metrics) of different VLN models, including DUET (Chen et al. 2022b), DSRG (Wang et al. 2023a), HAMT (Chen et al. 2021) and our SUSA. To ensure a fair comparison across all methods, we performed single-step forward inference with a batch size of 8, an instruction length of 44, and 6 exploration map nodes. Compared to the baseline DUET, our approach introduces spatial and semantic environmental information, which inevitably increasing computational cost. However, benefiting from the partial pretraining strategy and a shared panorama encoder for both the depth and RGB environmental information, our SUSA architecture notably enhances agent navigation performance with modest computational resources. The frozen BLIP-2 and CLIP models provide the SUSA agent with off-the-shelf textual semantics and are excluded from the training or inference.

C Qualitative Examples

Failure cases. We provide an in-depth examination of failure cases, aiming to offer valuable insights for future model improvements. 11 displays the difference between the navigation trajectory predicted by the proposed SUSA and the ground truth trajectory. We found that, although textual semantics can provide the agent with a richer understanding, it may introduce ambiguity in certain scenarios. Concretely, when two identical salient landmarks appear in different scenes (e.g., the staircase and bathroom in 11), the agent

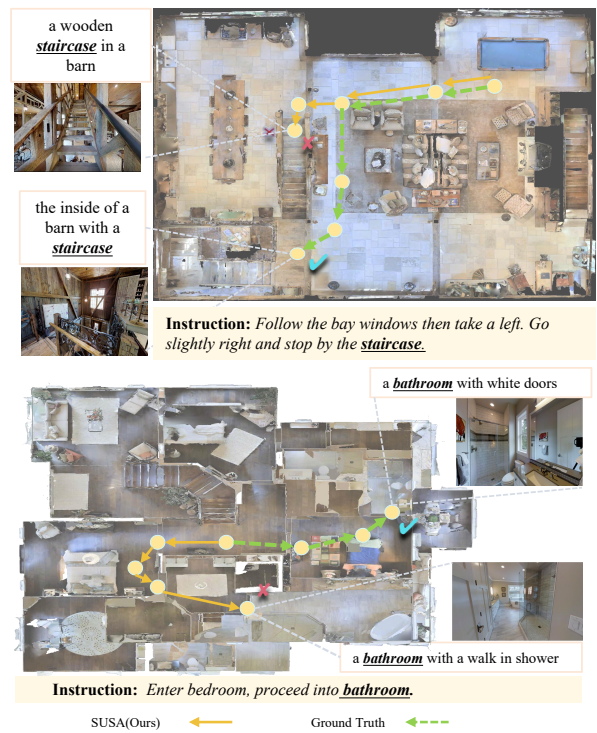


Figure 11: Top-down trajectories visualization of failed cases. Partial views of final stop position and corresponding landmark captions are also provided.

may struggle to distinguish the correct navigable node, leading to erroneous navigation decisions.

More Qualitative Examples. We further visualize first-person navigation trajectories on the R2R validation unseen split, as illustrated in Fig. 12.

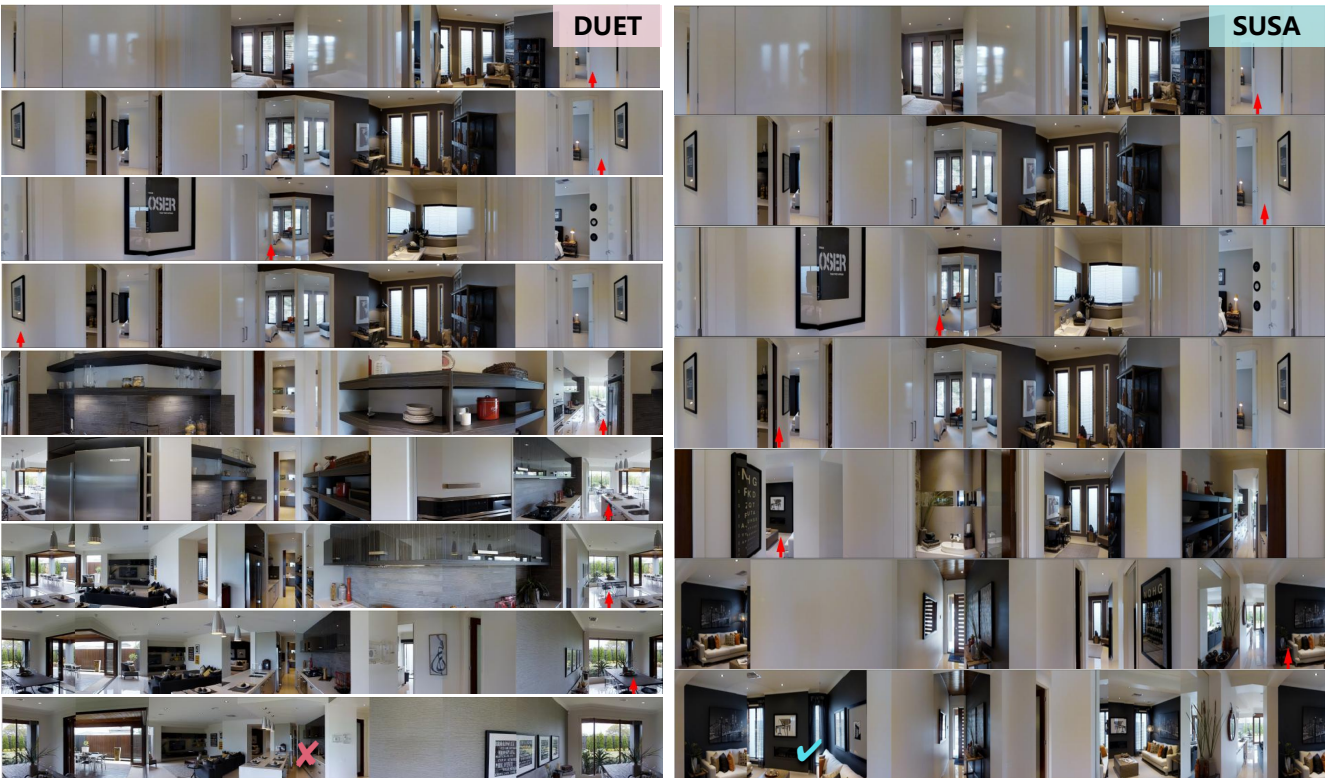
D Limitations and Future Work

As previously mentioned, when an agent encounters the same landmark at different navigable points, it may struggle to make confident navigation decisions, leading to failures. To address this limitation, 1) our future research will explore adjusting the confidence levels associated with different environmental representations to help the agent make more accurate and reliable predictions. 2) Beyond landmarks, we will construct direction-related textual semantics (e.g., “past,” “turn left”) to better model the spatial relationships between actions in instructions and the environmental layout or historical exploration maps.

In the future, we also intend to explore the generalizability of our approach, which hierarchically integrates richer representations from multiple perspectives, in embodied tasks such as continuous navigation and embodied question answering. Additionally, given the complexity of VLN tasks, current mainstream VLN frameworks are often intricate and cumbersome, with a wide variety of evaluation metrics that are difficult to balance. Ongoing research in the future is expected to develop more lightweight VLN model architectures and comprehensive evaluation metrics.



Instruction: Turn around and go to the left. Turn right and cross through the kitchen. At the end of the hallway stop.



Instruction: Go straight and make a sharp left then go towards the living room where you will see a photo frame of the nyc skyline

Figure 12: First-person trajectory visualizations of DUET (left) and our SUSA (right), with the corresponding instructions provided below. Red arrows indicate the next selected viewpoint from current position.